JOURNAL OF THERMOPHYSICS AND HEAT TRANSFER
Vol. 14, No. 2, April–June 2000

Measurement of Shock Standoff Distance for Sphere in Ballistic Range

Satoshi Nonaka,* Hiroyasu Mizuno,* Kazuyoshi Takayama,† and Chul Park‡
Tohoku University, Sendai 980-8577, Japan

The shock standoff distance for a sphere is measured in a ballistic range in the intermediate hypersonic regime. The measurement is made for hemispheres of nose radius of 7, 14, and 15 mm, flight speeds between 2.44 and 3.85 km/s, and ambient pressures between 5.6×10^2 and 2.0×10^4 Pa. The shock waves and flowfields over the spheres are visualized by shadowgraph or schlieren method using a pulse Nd-YAG laser as light source. The effect of contamination in the test air on the standoff distance was examined by using a turbo-molecular pump in setting the initial gas pressure. Shock standoff distances vary with the ambient pressure. Its variation from those in the ideal gas analysis clearly demonstrates the effect of the thermochemical nonequilibrium. The data are compared with the results of the previous investigation. The present data showed slightly larger standoff distance than those of previous experiment, indicating the effect of test gas contamination.

Nomenclature

R = radius of sphere
γ = specific heat ratio
Δ_{layer} = shock-layer thickness
Δ_s = shock standoff distance along the stagnation streamline
ρ = density

Introduction

DURING the atmospheric flight of space vehicles at a hypersonic speed, the air molecules in the shock layer are vibrationally excited, dissociated, and ionized. High-temperature real air absorbs the kinetic energy of molecules and thereby reduces the gas temperature and hence increases the density. As a result, the thickness of the shock layer is reduced. The real-gas effect drastically changes the pressure distribution over the vehicle from that predicted in ideal gas analysis and thereby its aerodynamic characteristics, i.e., lift, drag, and pitching moment should be determined by considering these effects.[1] To design an efficient hypersonic vehicle, these high-temperature real-gas effects must be accurately accounted.

The real-gas effects can be characterized fairly accurately in a thermochemical equilibrium state because equilibrium states are well understood.[2] When high-temperature flows are not in equilibrium, their characterizations become difficult and would be inaccurate because nonequilibrium of the chemical reactions in the high-temperature flows are not yet understood well. This is because not only the rates of relaxation of vibrational excitation and chemical reactions, but also the coupling mechanism between vibration and dissociation would dominantly govern the high-temperature flow characteristics.[3]

Presently, it is customary to predict the aerodynamic characteristics of a hypersonic vehicle using computational fluid dynamics (CFD). The high-temperature flow in thermochemical nonequilibrium associated with simultaneous dissociation and vibrational excitation can be handled in CFD by commonly introducing a two-temperature model that assumes a vibrational temperature among different molecules that is different from the translational temperature.[4,5] At high hypersonic speeds, i.e., at Mach numbers exceeding 15, oxygen molecules completely dissociate immediately behind the shock wave, and air becomes approximately a binary mixture of N_2 and O. Because this mixture has only one molecular species, flow properties can be characterized reasonably accurately using the two-temperature model. The model has already been validated for this high hypersonic speed range.[5]

In the intermediate hypersonic range from a Mach-number range from 8 to 15, hypersonic vehicles with airbreathing propulsion systems are planned. In this regime O_2 and NO molecules exist in substantial concentrations in addition to N_2. The vibrational temperatures of these three species cannot in general be the same. Interactions among the three vibrational modes of these species and their coupling with the translational mode would complicate the problem further. There is no assurance that the two-temperature model can adequately describe this flow regime. This is partly because experimental data are scarce in this speed range. Experiment is needed first to produce the reliable data for validation of CFD solutions in this speed range.[6,7]

Characteristics of hypersonic aerothermodynamics are studied experimentally using high-enthalpy shock tunnels or expansion tubes.[8–11] However, because chemical reactions are frozen in expanding regions, the flows in the test sections of such facilities generally contain vibrationally excited and dissociated gas species. The extent of such a chemically frozen state is not well known. Moreover, uncertainly concerning the freestream conditions and deviations from the undisturbed flow make the data unreliable.[1] Therefore, it is necessary to calibrate the measured data in such facilities before they can be used to validate the CFD solutions. For this purpose reliable data that can calibrate the flowfields must be collected by comparing flows over simple geometries. That is, reliable experimental data would serve not only for validating CFD solutions but also for calibrating a high-enthalpy facility itself.

One of the most appropriate reference quantities is the shock standoff distance over a sphere because the real-gas effects behind a detached shock wave significantly affect the shock standoff distance. Hypersonic flights achievable in a ballistic range should be capable of producing reliable data. In it a model is launched at hypersonic speed into quiescent gas so that the initial condition and the constitution of test gases is exactly controlled.[1,12]

Such measurement has been already made by Lobb in the 1960s (see Fig. 1).[13] As seen in Fig. 1, most of the data were taken at velocities above 4 km/s because this experiment was aimed at studying space vehicle reentry conditions. Presently, the data required

Presented as Paper 97-0563 at the AIAA 35th Aerospace Sciences Meeting, Reno, NV, 6–10 January 1997; received 14 June 1999; revision received 14 October 1999; accepted for publication 14 October 1999.

*Graduate Student, Department of Aeronautics and Space Engineering. Student Member AIAA.

†Professor, Shock Wave Research Center, Institute of Fluid Science. Member AIAA.

‡Professor, Department of Aeronautics and Space Engineering; currently Senior Research Scientist, Mail Stop 229-1, Thermosciences Institute, NASA Ames Research Center, Moffett Field, CA 94035-1000. Associate Fellow AIAA.

for the development of hypersonic airbreathing vehicles are the shock standoff distance in the strongly nonequilibrium region below 4 km/s. The purpose of the present study is to measure, in a ballistic range, the shock standoff distance for a sphere in the intermediate hypersonic regime.

One potential major source of error in the measurement of shock standoff distance is the pulse duration of the light source. This is because images of high-speed projectile become blurred over an irradiation time of the light source. Lobb's experiment was carried out by using a light source of relatively long pulse duration. A geometrical error is also introduced that is inversely proportional to the model size. The models used in Lobb's experiment had a diameter of 12.7 mm. Hence it is worthwhile to first confirm the accuracy of Lobb's data. In the present study a Nd-YAG laser of short pulse duration is used as light source for visualization. The model size is also larger than that used by Lobb. As a result, the potential error involved in the present optical measurement is much improved over those in Lobb's.

Test Facilities and Conditions

Ballistic Range Facility

The experiment was conducted in the ballistic range in the Shock Wave Research Center of the Institute of Fluid Science, Tohoku University. The facility is shown schematically in Fig. 2. The facility has been designed and constructed as a two-stage light gas gun and consists of a powder chamber, a 60-mm inside diameter (i.d.) pump tube 3 m in length, a high-pressure coupling, a 4-m-long launch tube, and a test chamber. Launch tubes of 14 and 30 mm i.d. were prepared and selected depending on model size. The test chamber has a 700 mm i.d. and is 1400 mm in length. The inside wall is cleaned after each shot so that contamination can be kept at a very low level.

The ballistic range is operated as follows. A high-density polyethylene piston is accelerated along the pump tube by high-pressure gas generated by the combustion of smokeless powder. The piston compresses a light gas, such as hydrogen or helium that fills the pump tube. The resulting high-pressure light gas ruptures the steel diaphragm, inserted between the pump tube and the high-pressure coupling and accelerates the projectile along the launch tube. The model is launched into the test chamber and eventually terminates on a steel bumper. The velocity of the model is measured by the time of flight of the model between two laser beams placed at 1 m distance apart in the test section.

Optical Arrangement

Shadowgraph and schlieren methods were used to determine the shock standoff distance. The former was used for tests in high-pressure conditions, and the latter was used in a low-pressure case because of high sensitivity. Figure 3 shows the optical arrangement of the schlieren method. To minimize blurring of the images of models moving at hypersonic speed, a light source of a extremely short duration is required. The available light source is a Nd-YAG laser of second harmonic wavelength of 532 nm with a 5-ns pulse duration and 770 mJ energy. For a 15-mm nose radius model moving at 4 km/s, the model moves only for 0.02 mm during a pulse. The relative error in the shock-layer thickness caused by the model movement is estimated to be no more than ±1%. The model successively passed two pressure ports installed 1 m apart along the launch tube near its exit. One of the pressure transducer output signals was used to trigger the laser. A delay circuit was used to determine the appropriate time interval.

The image of the model was recorded on a 100 × 125 mm sheet film AGFA-GEVAERT 10E56, which is sensitive to light at a relatively narrow region of wavelength around 560 nm. The luminescence generated at the shock layer and also during the impact of the model on the steel bumper produced a broadband spectra so that the present film is insensitive to it. The recorded photographic images were then magnified and digitized by processing them with an optical scanner. The shock standoff distance was deduced from the digitized data.

Test Conditions

The degree of thermochemical nonequilibrium is characterized by the Damköhler number. In a flow where two-body reactions are dominant, this parameter is proportional to the product of the freestream density ρ and the body radius R. Therefore, the chemical reaction processes in the shock layer around the stagnation point can be correctly simulated by reproducing the parameter ρR. The Reynolds number is proportional also to the product of density and

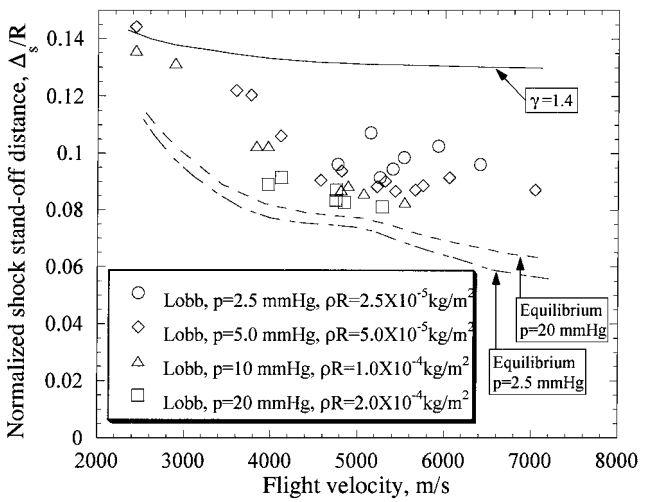

Fig. 1 Shock standoff distance for sphere measured by Lobb.[13]

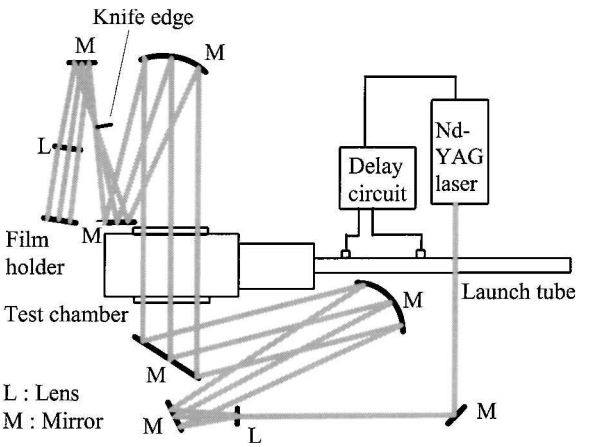

Fig. 3 Optical arrangement of schlieren method.

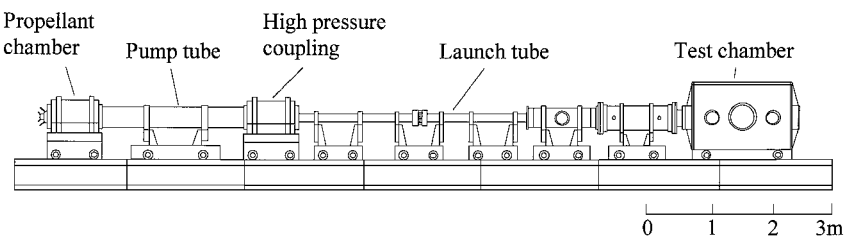

Fig. 2 Schematic of the ballistic range in the Shock Wave Research Center.

characteristic length. In hypersonic similarity, not only the Mach number M but also the Reynolds number Re should be equaled, which eventually results in making ρR identical. ρR is hence called the binary scaling parameter. Therefore, ballistic range experiments can reproduce the Damköhler number and also the Reynolds number of various flight conditions simply by changing the model size and the test gas pressure. To measure shock standoff distances for a sphere, values of ρR of 1.0×10^{-4}, 2.0×10^{-4}, 4.0×10^{-4}, and 1.7×10^{-3} kg/m^2 are chosen by changing the test gas pressure from 5.6×10^2 to 2.0×10^4 Pa and the model nose radius R from 7 to 15 mm. The present models were made of AZ-31-F magnesium alloy and machined in the shape of hemisphere cylinders with radius of 7, 14, and 15 mm. The corresponding weights of each were 4.0, 10.0, and 18.7 g, respectively.

In the present experiments smokeless powder between 60- and 100-g weight was used. The high-density polyethylene piston contained a copper cylinder with a total weight of about 1550 g. The diaphragms inserted between the powder chamber and the high-pressure coupling were 1.0-mm-thick stainless steel and 2.0- or 2.5-mm-thick steel, respectively. The helium pressure in the pump tube was between 6.9×10^5 and 7.8×10^5 Pa, and the gas temperature in the test section was about 293 K. To purge the contamination in the test section, first it was evacuated by a turbo-molecular pump to below 0.1 Pa. Uncontaminated dry air was then supplied. The test-section pressure was measured by a mercury manometer.

Results and Discussions

Figures 4 and 5 show typical examples of shadowgraph and schlieren photographs obtained for flow over a 15-mm-nose-radius model. Figure 4 is for a velocity of 2.93 km/s, $\rho R = 1.0 \times 10^{-4}$ kg/m^2, and Fig. 5 is for 2.61 km/s, $\rho R = 4.0 \times 10^{-4}$ kg/m^2. The shape of the detached shock wave can be clearly seen in both images.

In Fig. 6 the shock standoff distances measured from the photographs are plotted along with the data reported by Lobb.[13] The ordinate is the shock standoff distance normalized by the nose radius Δ_s / R, and the abscissa is the projectile velocity in m/s. The results obtained from the numerical solutions of Van Dyke and Gordon[14] along with the Hilsenrath et al.[15] tables are also shown in Fig. 6. The upper solid curve designates the analytical results for an ideal gas of $\gamma = 1.4$ corresponding to $\rho R = 0$. The lower ones give the predicted Δ_s / R in chemical equilibrium at two different ambient pressures corresponding to $\rho R = \infty$. The domain between these two sets of curves represents the nonequilibrium region for finite ρR. Values of the present data are summarized in Table 1. In addition to the model movement during the pulse duration, the resolution in

Table 1 Shock standoff distances and test conditions

Binary scaling parameter ρR, kg/m^2	Flight velocity, m/s	Model radius, mm	Normalized shock standoff distance	Error, ±%
1.0×10^{-4}	2470	15	0.1408	1.15
	2630	14	0.1350	3.15
	2670	14	0.1345	2.68
	2930	15	0.1372	1.10
	3570	7	0.1251	3.96
	3850	7	0.1212	1.82
2.0×10^{-4}	2540	15	0.1383	1.58
	2560	14	0.1370	1.90
	2630	14	0.1332	1.84
	3150	15	0.1287	4.97
	3250	7	0.1277	2.58
	3360	7	0.1285	2.53
	3640	7	0.1137	2.99
4.0×10^{-4}	2500	15	0.1324	2.57
	2610	15	0.1328	1.05
	3190	7	0.1187	3.79
	3370	7	0.1163	1.63
	3490	7	0.1129	1.33
1.7×10^{-3}	2440	15	0.1278	2.19
	2560	14	0.1243	2.09
	3160	7	0.1040	4.31

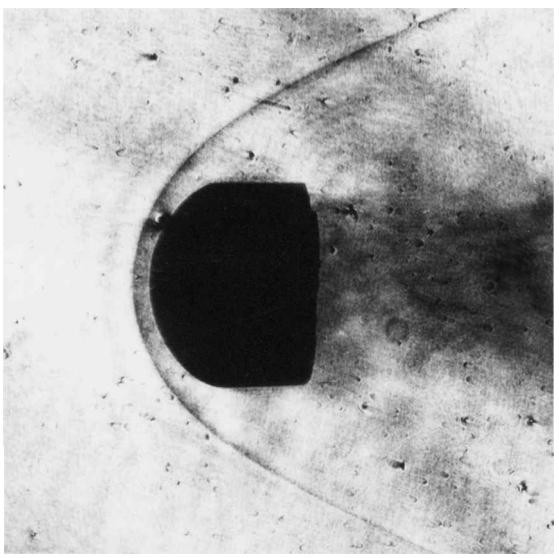

Fig. 4 Schlieren of a flowfield over a 15-mm nose-radius sphere model flying at 2.93 km/s: initial pressure = 560 Pa.

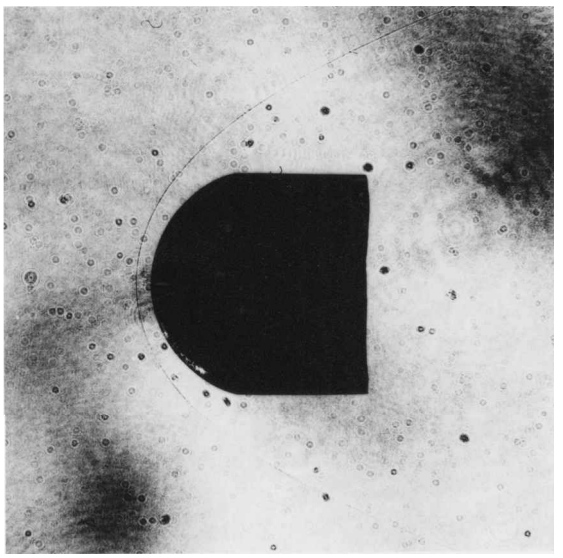

Fig. 5 Shadowgraph of a flowfield over a 15-mm nose-radius sphere model flying at 2.61 km/s: initial pressure = 2240 Pa.

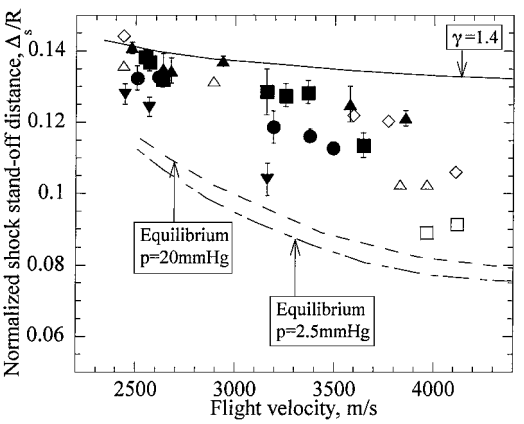

Fig. 6 Normalized shock standoff distance for sphere: ▲, present, $\rho R = 1.0 \times 10^{-4}$ kg/m^2; ■, present, $\rho R = 2.0 \times 10^{-4}$ kg/m^2; ●, present, $\rho R = 4.0 \times 10^{-4}$ kg/m^2; ▼, present, $\rho R = 1.7 \times 10^{-3}$ kg/m^2; ◇, Lobb,[13] $\rho R = 5.0 \times 10^{-5}$ kg/m^2; △, Lobb,[13] $\rho R = 1.0 \times 10^{-4}$ kg/m^2; and □, Lobb,[13] $\rho R = 2.0 \times 10^{-4}$ kg/m^2.

reading shock position on the film causes some possible errors. As the result, the averaged error of the normalized shock standoff distance so far measured is about ±2%.

As shown in Fig. 6, the present data exhibit nonequilibrium effects. In the case of binary scaling parameter of $\rho R = 1.0 \times 10^{-4}$ kg/m^2, measured data lie close to the theoretical curve for an ideal gas. At low initial pressures chemical reactions behind a shock wave are generally frozen. As a result, the shock standoff distance nearly agrees with an ideal gas value. However, for $\rho R = 2.0 \times 10^{-4}$ and 4.0×10^{-4} kg/m^2 experimental points are located in the middle of the nonequilibrium regime. This indicates that nonequilibrium effects become significant even in the intermediate hypersonic speed range while keeping ρR constant. As the value of ρR is increased, the shock standoff distance approaches the predicted equilibrium values.

Comparing the present results with Lobb's data,[13] we found the present experiments gave larger standoff distances that are closer to the frozen value and in a higher velocity region. Figure 7 shows the comparison between the present data and Lobb's ones in the case of the binary scaling parameter of $\rho R = 1.0 \times 10^{-4}$ kg/m^2. The curve fitted by Lobb is also shown. Presumably this discrepancy may be attributable to the contamination of the test gas in Lobb's experiment because of the use of an oil-sealed rotary vacuum pump or a diffusion pump. To reconfirm this effect, the shock standoff distance was measured with the test gas evacuated by an oil-sealed rotary vacuum pump. Figure 8 compares normalized shock standoff distances obtained both with the test gas arranged by an oil-rotary vacuum pump and by a turbo-molecular pump. The effects of oil vapor contamination appear to reduce the shock standoff distance at the initial pressure by 7–15% in comparison to the uncontaminated air. The contaminant molecules have relatively large molecular weights and are vibrationally excited and dissociated behind a shock wave. This effect absorbs heat so that the shock standoff distance is shortened.

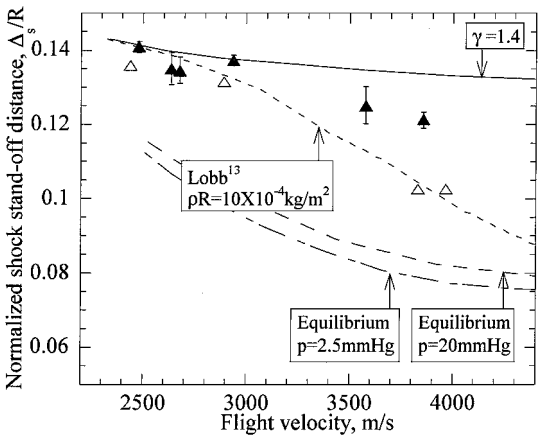

Fig. 7 Comparison between the present and Lobb's data[13] for $\rho R = 10 \times 10^{-4}$ kg/m^2: ▲, present, $\rho R = 1.0 \times 10^{-4}$ kg/m^2; and △, Lobb,[13] $\rho R = 1.0 \times 10^{-4}$ kg/m^2.

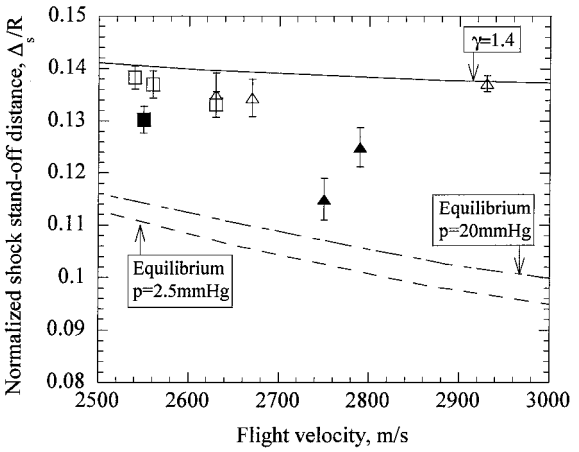

Fig. 8 Effect of oil vapor on shock standoff distance: △, uncontaminated, $\rho R = 1.0 \times 10^{-4}$ kg/m^2; □, uncontaminated, $\rho R = 2.0 \times 10^{-4}$ kg/m^2; ▲, contaminated, $\rho R = 1.0 \times 10^{-4}$ kg/m^2; and ■, contaminated, $\rho R = 2.0 \times 10^{-4}$ kg/m^2.

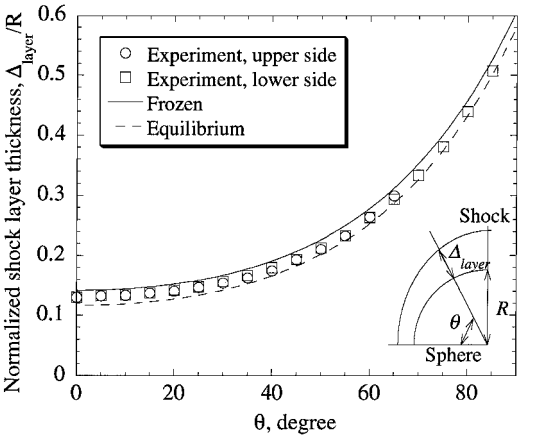

Fig. 9 Normalized shock-layer thickness over a 15-mm-nose-radius sphere: flight velocity = 2.61 km/s, initial pressure = 2240 Pa.

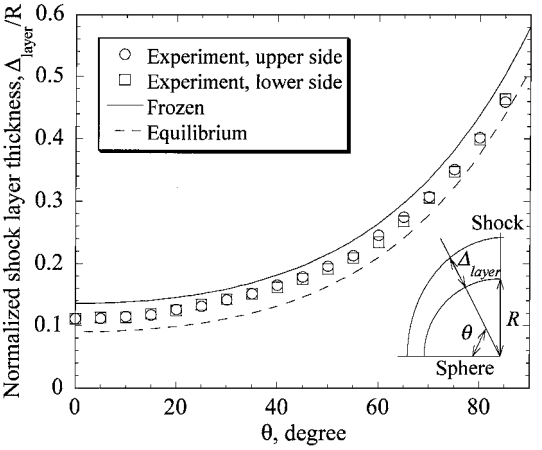

Fig. 10 Normalized shock-layer thickness over a 7-mm-nose-radius sphere: flight velocity = 3.49 km/s, initial pressure = 4850 Pa.

In Figs. 9 and 10 the shock shapes are presented in the form of the normalized shock-layer thickness Δ_{layer}/R as a function of the polar angle measured from the center axis. Figure 9 shows a 15-mm nose radius model moving at 2.61 km/s and with the initial pressure = 2240 Pa. Figure 10 is for a 7-mm-nose-radius model at 3.49 km/s, and the initial pressure = 4850 Pa. For these conditions the binary scaling parameter $\rho R = 4.0 \times 10^{-4}$ kg/m^2. Figures 9 and 10 also show the Δ_{layer}/R values measured in the upper and lower sides of the axis of symmetry. Numerical values for frozen and equilibrium flow are also plotted for comparison. The frozen values were calculated using a two-temperature code,[7] in which the chemical reaction and vibrational excitation were prohibited to obtain frozen solution. The equilibrium values are obtained by an existing equilibrium flow solver.[16]

In Figs. 9 and 10 the Δ_{layer}/R values from the upper and lower sides of the photograph agree well with each other. This would indicate that the procedure of determining shock standoff distance was conducted accurately. The difference of shock-layer thickness between frozen and equilibrium flows become larger at the higher velocity. The measured Δ_{layer}/R values lie between the frozen and equilibrium limits and approach the equilibrium values toward the downstream, as expected.

Conclusions

Shock standoff distances for a sphere have been measured using a ballistic range, and the following conclusions were drawn. The

difference in shock standoff distances between frozen, nonequilibrium, and equilibrium flows are clearly recognized even in intermediate hypersonic speed range. The shock standoff distances obtained in the present experiment are larger than previous values obtained by Lobb. This is attributable to the level of oil vapor contamination in the test gas of the previous study. The measured shock-layer thicknesses are in the nonequilibrium regime and approach the equilibrium shapes toward the downstream.

Acknowledgments

The authors would like to thank K. Sawada of Tohoku University for his valuable suggestions and comments. The authors also wish to thank O. Onodera, M. Adachi, H. Ojima, T. Ogawa, and K. Okano of Shock Wave Research Center, Tohoku University, for their help in conducting the present experiments. M. Furudate, a graduate student at Tohoku University, helped conduct the present calculations.

References

[1]Park, C., "Experimental Simulation and Evaluation of Chemical Effects," *Aerothermochemistry for Hypersonic Technology*, von Kármán Inst. for Fluid Dynamics Lecture Series, 1995-4, edited by G. S. R. Sama, 1995, pp. 1–57.

[2]Vincenti, W. G., and Kruger, C. H., Jr., *Introduction to Physical Gas Dynamics*, Wiley, New York, 1965, pp. 152–196.

[3]Park, C., *Nonequilibrium Hypersonic Aerothermodynamics*, Wiley, New York, 1990, pp. 43–118.

[4]Park, C., "Assessment of Two-Temperature Kinetic Model for Dissociating and Weakly-Ionizing Nitrogen," *Journal of Thermophysics and Heat Transfer*, Vol. 2, No. 1, 1988, pp. 8–16.

[5]Park, C., "Assessment of Two-Temperature Kinetic Model for Ionizing Air," *Journal of Thermophysics and Heat Transfer*, Vol. 3, No. 3, 1989, pp. 233–244.

[6]Park, C., "Validation of CFD Codes for Real-Gas Regime," AIAA Paper 97-2530, June 1997.

[7]Furudate, M., Nonaka, S., and Sawada, K., "Behavior of Two-Temperature Kinetic Model in Intermediate Hypersonic Regime," AIAA Paper 99-0223, Jan. 1999.

[8]Hornung, H. G., "Non-Equilibrium Dissociating Nitrogen Flow over Spheres and Circular Cylinders," *Journal Fluid Mechanics*, Vol. 64, Pt. 4, 1974, pp. 725–736.

[9]Hornung, H. G., and Wen, C. Y., "Nonequilibrium Dissociating Flow over Spheres," AIAA Paper 95-0091, Jan. 1995.

[10]Spurk, J. H., "Experimental and Numerical Nonequilibrium Studies," *AIAA Journal*, Vol. 8, No. 6, 1970, pp. 1039–1045.

[11]Miller, C. G., III, "Shock Shapes on Blunt Bodies in Hypersonic-Hypervelocity Helium, Air, and CO_2 Flows, and Calibration Results in Langley 6-Inch Expansion Tube," NASA TN D-7800, Feb. 1975.

[12]Sharma, S. P., and Park, C., "Survey of Simulation and Diagnostic Techniques for Hypersonic Nonequilibrium Flows," *Journal of Thermophysics and Heat Transfer*, Vol. 4, No. 2, 1990, pp. 129–142.

[13]Lobb, R. K., "Experimental Measurement of Shock Detachment Distance on Sphere Fired in Air at Hypervelocities," *The High Temperature Aspects of Hypersonic Flow*, edited by W. C. Nelson, Pergamon, New York, 1964, pp. 519–527.

[14]Van Dyke, M. D., and Gordon, H. D., "Supersonic Flow Past a Family of Blunt Axisymmetric Bodies," NASA TR R-1, 1959.

[15]Hilsenrath, J., Beckett, C. W., Benedict, W. S., Fano, L., Hoge, H. J., Masi, J. F., Nuttall, R. L., Touloukian, Y. S., and Woolley, H. W., *Tables of Thermodynamic and Transport Properties of Air, Argon, Carbon Dioxide, Carbon Monoxide, Hydrogen, Nitrogen, Oxygen, and Steam*, Pergamon, New York, 1960, pp. 14–74.

[16]Sawada, K., and Dendou, E., "Validation of Hypersonic Equilibrium Flow Calculations Using Ballistic-Range Data," AIAA Paper 97-0344, Jan. 1997.